Effective Targeting of the Tumor Microenvironment for Cancer Therapy

PING JIANG[1], XIAOMING LI[1], CURTIS B. THOMPSON[1], ZHONGDONG HUANG[1], FLAVIO ARAIZA[1], RYAN OSGOOD[1], GE WEI[1], MARC FELDMANN[2], GREGORY I. FROST[1] and H. MICHAEL SHEPARD[1]

[1]Halozyme Therapeutics, San Diego, CA, U.S.A.;
[2]Kennedy Institute of Rheumatology, Nuffield Department of Orthopaedics,
Rheumatology and Musculoskeletal Sciences, University of Oxford, London, U.K.

Abstract. *Background: The tumor microenvironment is an emerging source of novel therapeutic targets in cancer. The glycosaminoglycan hyaluronan (HA) accumulates in 20-30% of tumors and is often associated with poor prognosis. Materials and Methods: We developed a digitized, semiquantitative scoring system for tumor-associated HA content, then grouped tumors (from animal models or patients) according to the degree of HA accumulation (HA+1,2,3). The antitumor response to HA-depletion by pegylated PH20 hyaluronidase (PEGPH20) was then characterized as a function of HA accumulation. Results: Semiquantitative grouping of tumors demonstrated that HA accumulation predicts the response of tumors in animal models to PEGPH20. Prospective analysis of HA content was used to predict response to PEGPH20 of squamous cell-type explants from patients with non-small cell lung cancer in nude mice. Conclusion: Measurement of HA is a viable biomarker approach for predicting antitumor response in animal models to the HA-depleting agent, PEGPH20.*

Hyaluronan (HA) is a glycosaminoglycan component of the extracellular matrix (ECM), which accumulates in many malignant and inflammatory disease conditions (1, 2). In cancer, the accumulation of HA in the tumor microenvironment (TME) has been associated with more aggressive malignancy both in preclinical models and in patients (3). The contribution of HA to tumor progression is multifactorial, as a result of its

Correspondence to: H. Michael Shepard, Ph.D., Halozyme Therapeutics, 11388 Sorrento Valley Road, San Diego, CA 94121, U.S.A. Tel: +858 7948889, Fax: +858 7048311, e-mail: mshepard@halozyme.com

Key Words: Tumor stroma, hyaluronan, hyaluronidase, PEGPH20, biomarker, microenvironment.

interactions with and cross-linking of other matrix components and cellular receptors, which perpetuate the protumorigenic TME (4-8). Accumulation of HA within a tumor focus interferes with cell–cell contact, promotes epithelial–mesenchymal transition, recruits tumor-associated macrophages and is associated with tumor drug resistance (8-10). Recently, HA was shown to promote the development of regulatory T-cells, perhaps promoting immune tolerance to cancer cells (11). The best characterized signal transducing molecules associated with HA are *CD44* and receptor for HA-mediated motility (*RHAMM*), both of which are p53-regulated genes linked to a role of HA in tumor progression (12, 13). The accumulation of HA in tumor foci contributes to a dramatic pressure disequilibrium between the tumor and surrounding tissue(s), largely due to the ability of HA to expand its solvent domain by coordinating at least three water molecules per disaccharide unit (14-16). HA levels can be increased by growth factors, cytokines and chemokines and increased HA accumulation itself is associated with expression of markers of disease progression (17-19). Many HA-associated biomechanical effects, such as elevated interstitial fluid pressure (IFP), can be reversed in animal tumor models following enzymatic depletion of HA with systemically administered pegylated PH20 hyaluronidase (PEGPH20) (20). Depletion of HA from an HA-rich TME leads to altered biochemical properties of the tumor, including reduced IFP, increased vascular perfusion, and increased tumor-specific accumulation of chemotherapy (20). These data suggest that the distinct biomechanical properties of disease foci which are characterized by high levels of HA create a specialized structure (*e.g.* a desmoplastic tumor) which in itself may be a novel target for therapy of multiple diseases.

The current work shows that tumor HA content can be measured semiquantitatively and used as a biomarker to predict tumor progression in experimental animal models. Gene expression array analysis and bromodeoxyuridine (5-bromo-2'-deoxyuridine, BrdU)-labeling *in vivo* were used to initially characterize the mechanism(s) of tumor response to PEGPH20.

Table I. *Quantitation of hyaluronan (HA) production, pericellular matrix (PM) formation, hyaluronan synthase (HAS) and hyaluronidase (HYAL) expression in tumor cell lines.*

Tumor cell line	PM[1] (μm^2)	HA in CM[2] (ng/ml)	HAS mRNA isoform[4]			Hyaluronidase isoform mRNA	
			HAS1	HAS2	HAS3	HYAL1	HYAL2
4T1	1552.00	473.83	NE	NE	NE	NE	NE
MDA-MB-231/HAS2[5]	1088.55	372.23	2.48	19.90	0.09	0.14	0.53
PC3	1072.20	294.45	1.41	0.34	6.32	0.14	1.19
DU-145/HAS2	981.00	707.22	1.08	7.81	0.65	0.34	1.04
BxPC3	967.20	467.12	1.00	1.00	1.00	1.00	1.00
MDA-MB-231 WT	770.45	256.91	3.39	0.54	0.05	0.13	0.64
MatLyLu	760.55	265.91	NE	NE	NE	NE	NE
AsPC-1	524.20	66.47	1.87	1.65	1.28	0.81	1.91
DU-145 WT	252.10	41.79	1.01	0.03	1.51	0.17	0.70
MIA PaCa-2	129.40	0.00	0.46	0.00	0.04	0.28	0.72
p-value[3]	–	0.0029	0.23	0.34	0.71	0.66	0.36

NE: Not evaluated. PM; [1]Assessed *via* particle exclusion assay as described in the Materials and Methods section. [2]Mean in culture media (n=3, independent cultures). [3]Spearman correlation coefficient test. [4]*HAS* and *HYAL* expression determined by real-time RT-PCR. Ct values were normalized by glyceraldehyde 3-phosphate dehydrogenase (GAPDH) mRNA and the fold differences are relative to mRNA expression of the same protein in BxPC3 pancreatic cancer cells. [5]HAS-2 over-expressing cells were prepared as described in the Materials and Methods section.

Materials and Methods

Cell culture. Cell lines (listed in Table I) were obtained from the American Type Culture Collection (ATCC, Manassas, VA, USA) and grown in recommended culture medium. MDA-MB-231/Luc cells were purchased from Caliper Lifescience Inc. (Hopkinton, MA, USA) and grown in RPMI containing 10% fetal bovine serum (FBS).

Establishment of Hyaluronan Synthase (HAS)2-transfected tumor cell lines. To generate HAS2 retrovirus, the *N*-terminal His6-tagged h*HAS2* cDNA was inserted into the *Avr*II and *Not*I sites of pLXRN (Clontech, Mountain View, CA, USA), which includes the neomycin resistance gene to create pLXRN-hHAS2. The virus titer was determined by a quantitative polymerase chain reaction (qPCR) method (Clontech). To establish cell lines with HAS2 expression, 70% confluent cancer cells were incubated at a 60:1 to 6:1 ratio with retrovirus in Dulbecco's Modified Eagle Medium (DMEM) (Mediatech, Manassas, VA USA) containing 10% FBS for 72 h. The cultures were maintained in selective medium containing 200 μg/ml of the antibiotic Geneticin™ (G418) (Invitrogen, Carlsbad, CA, USA).

Quantification of HAS1, HAS2, HAS3, Hyaluronidase (HYAL)1 and HYAL2 mRNAs. RNA was extracted from cell pellets using an RNeasy® Mini Kit (Qiagen GmbH, Hilden, Germany). First-strand cDNA synthesis and real-time PCR using gene-specific primers were obtained from BATJ, Inc. (San Diego, CA, USA) (Table II). Specific gene expression from each sample was calculated by normalizing with the internal housekeeping gene glyceraldehyde 3-phosphate dehydrogenase (*GAPDH*) and relative values were plotted.

Particle exclusion assay. To visualize HA pericellular matrices (PMs) *in vitro*, particle exclusion assays using fixed red blood cells were performed as described elsewhere (20). Particle exclusion area and cell area were measured using the formula: PM area calculated as (matrix area – cell area), and expressed as μm^2.

Quantification of hyaluronic acid in tissue culture. Tumor cells were seeded at 1×10^6 cells in 75 cm^2 flasks and incubated for 24 h. Tissue culture supernatants were harvested for quantitation of HA using an enzyme-linked hyaluronan binding protein (HABP) sandwich assay (R&D Systems, Minneapolis, MN, USA) following the manufacturer's instructions.

Histochemical staining of HA in tissue. Tissue microarrays (TMA) used in this study were purchased from BioMax US Inc. (Rockville MD, USA). Xenograft tumor tissues were from multiple *in vivo* studies archived in house. Histochemical methods were used to localize HA in tissue as described elsewhere (20, 21), with some modifications. Some sections were stained with biotinylated (b)HABP that had been pre-treated with rHuPH20 (1000 U/ml) in piperazine-N,N'-bis(2-ethanesulfonic acid, PIPES) buffer [25 mM PIPES, 70 mM NaCl, 0.1% bovine serum albumin (BSA), pH 5.5] at 37°C for 1 h before staining for HA, and served as negative controls.

Semiquantification of HA staining. An Aperio T2 Scanscope (Aperio, Vista, CA, USA) was used to generate high-resolution images of tissue sections and TMAs. Images were quantitatively analyzed with Aperio Spectrum software using a pixel count algorithm for brown color (HA) count. Tissue in the sections or arrays with less than 10% of tumor cells or more than 50% of necrotic tissue was excluded for the evaluation. PC3 (HA+3) xenograft tumor tissues were used as a positive control. A ratio of strong positively (brown) stained area to the sum of the total stained area was calculated and scored as +3, +2, +1 or 0 when the ratio was more than 25%, 10-25%, less than 10% or 0, respectively.

In vivo BrdU incorporation assay. Mice with PC3 tumor xenografts were treated with vehicle or PEGPH20 twice weekly for two weeks. The mice were administered 10 mg/kg BrdU, (Invitrogen) *i.p.* the day before study termination. Tumors were excised, fixed in 10%

Table II. *Primers used in this study.*

Gene	Forward primer	Reverse primer
HAS1	5'-TACAACCAGAAGTTCCTGGGG-3'	5'-CTGGAGGTGTACTTGGTAGC-3'
HAS2	5'-GTATCAGTTTGGTTTACAATC-3'	5'-GCACCATGTCATATTGTTGTC-3'
HAS3	5'-CTTAAGGGTTGCTTGCTTGC-3'	5'-GTTCGTGGGAGATGAAGGAA-3'
HYAL1	5'-GTGCTGCCCTATGTCCAGAT-3'	5'-ATTTTCCCAGCTCACCCAGA-3'
HYAL2	5'-TCTACCATTGGCGAGAGTG-3'	5'-GCAGCCGTGTCAGGTAAT-3'
GAPDH	5'-TGCACCACCAACTGCTTAGC-3'	5'-GGCATGGACTGTGGTCATGAG-3'

Primers used in this study were derived from Udabage *et al*. (51).

buffered formalin and embedded in paraffin. Tissues were cut into 5 µm sections, and cell proliferation was assessed after staining with the Invitrogen BrdU Staining Kit.

Localization and semiquantification of collagen in tumor tissue. Paraffin-embedded tumor tissues were cut, dewaxed, and rehydrated in deionized (DI) water. Antigen retrieval was processed by heating slides in EDTA buffer at pH 8.0, at 100˚C for 25 min. Slides were rinsed in phosphate buffer solution with Tween-20 (PBS-T), blocked with 2% normal goat serum in 2% PBS/BSA for 30 min, followed by incubation with rabbit polyclonal anti-collagen type 1 antibody (1:200 dilution, Abcam, Cambridge, MA, USA) for 2 h at room temperature (RT). The sections were then incubated in Texas red-tagged goat anti-rabbit IgG (1:200 dilution, Vector Laboratories, Burlingame, CA USA) for 1 h at RT, and counterstained and mounted with ProLong® Gold antifade reagent with 4',6-diamidino-2-phenylindole (DAPI) (Invitrogen). Micrographs were captured under a Zeiss Axioskop microscope coupled with an RT3 camera (Diagnostic Instruments, Sterling Heights, MI, USA). Five random fields from each section were analyzed for collagen-positive intensity using Image-Pro plus program (MediaCybernetics, Bethesda, MD, USA).

Xenograft tumor models. Tumor-inoculated six- to eight-week-old nu/nu (Ncr) athymic nude mice were housed in micro-isolator cages, in an environmentally controlled room on a 12-h light/12-h dark cycle, and received sterile food and water *ad libitum*. Tumor volumes were determined and tumor growth inhibition (TGI) was calculated as described elsewhere (20). All animal studies were conducted in accordance with approved Institutional Animal Care and Use Committee (IACUC) protocols. Statistical analysis of differences in tumor volumes between the control and treatment groups one day after the last treatment dose was performed using a one-way ANOVA test with *p*-value of $p \le 0.05$ defined as statistical significance.

cDNA array analysis of stromal gene expression in PC3 xenograft tumor tissue. NCR *nu/nu* mice bearing PC3 tumors were treated with one dose of vehicle or PEGPH20. Animals were euthanized 8 and 48 h post-dose, tumor tissues were excised in sterile condition, and snap frozen in liguid nitrogen (Ln2) (Airco Gas and Gear, San Marcos, CA, USA). Total RNA was isolated and mRNA profiling studies were performed by Assuragen using the Affymetrix Mouse 430 2.0 Array (Affymetrix, Santa Clara, CA, USA).

Derivation of patient non-small cell lung cancer (NSCLC) tumor explants and treatment with PEGPH20. Tumor biopsies were obtained from patients with NSCLC, then maintained subcutaneously

in nude mice. Seed tumors (500-700 mm^3) were minced into 3×3×3 mm fragments; one fragment was subcutaneously implanted into the right rear flank of a Balb/c nude mouse. The tumor volumes were determined by caliper measurements of the greatest longitudinal diameter (length) and the greatest transverse diameter (width). Tumor volumes were estimated using the calculation of 1/2(length × width^2). The animals were randomized into two groups when the average tumor size reached 500 mm^3 (range 300-600 mm^3). For therapy, animals were treated with vehicle or PEGPH20 at 4.5 mg/kg twice weekly for five doses. The percentage TGI and statistical analysis were performed as described above.

Statistical analysis. Statistical analyses were performed using JMP® 8 program (JMP, Cary, NC, USA). Two-way ANOVA was used to compare multiple variances. Spearman correlation coefficients and Wilcoxon tests were used to evaluate the relationships between HA expression and response to PEGPH20 treatment.

Results

HA-binding protein detection of HA in conditioned media predicts HA PM formation. In order to determine whether HA accumulation in the TME is related to the efficacy of therapeutic modalities that deplete tumoral HA, it was first necessary to document an assay that could predict the ability of HA-synthesizing tumor cells to form a PM. Previous work has shown that HA produced by cells in culture is heterogeneous in amount, size, and ability to form aggrecan-mediated pericellular matrix (3). HABP-based assays are preferable to other methods (22) for measuring HA as a TME biomarker because HABPs will detect biologically relevant HA with a minimum size of 15 disaccharides (*N*-acetylyglucose-glucuronic acid), which is likely to be the smallest size that can cross-link other matrix components or impact tumor IFP (23). Monolayer cultures of ten cell lines were tested for PM formation (Table I). The ability of each cell line to form a PM was then compared with the measurement of soluble HA in conditioned media *in vitro* (measured by an HABP sandwich ELISA-like assay), as well as with the mRNA expression of HAS1, -2, -3 and HYAL1 and -2 (Table I). The concentration of HA in conditioned media as determined by the ELISA-based detection assay

Table III. *Comparison of tumor growth inhibition (TGI) by recombinant human hyaluronidase (rHuPH20) and pegylated recombinant human PH20 hyaluronidase (PEGPH20).*

Agent	Dose[1]	TGI	p-Value[2]
Vehicle			
PEGPH20	1 mg/kg	32±11%	<0.05
rHuPH20	0.33 mg/kg	8±12%	NS

NS, Not studied; [1]PEGPH20 (~33,000 units/mg) and rHuPH20 (~100,000 units/mg)-treated animals received the same number of units of enzyme. [2]Animals bearing H1975 non-small cell lung cancer xenografts (8 per group) were treated with vehicle or hyaluronidase as described in the Materials and Methods section.

Table IV. *Tabulated list of relative tumor hyaluronan (HA) intensity and corresponding tumor growth inhibition (TGI).*

Model	Tumor type (source)	Mean HA pixels (%)	TGI (%)
Du145/VO	Prostate (H)	3.50	0
MDA-MB-231	Breast (H)	4.59	0
SKOV3	Ovarian (H)	4.87	0
MDA-MB-231/Luc	Breast (H)	6.97	23
MDA-MB-231/ Luc/HAS2	Breast (H)	11.18	43
AsPc-1	Pancreatic (H)	15.15	18
MIA PaCa-2	Pancreatic (H)	17.08	24
LUM 330	Lung (H)	17.70	44
4T1	Breast (M)	19.45	45
BxPC3	Pancreatic (H)	20.50	61
MatLyLu	Prostate (R)	24.00	34
PC3	Prostate (H)	27.27	65
DU-145/HAS2	Prostate (H)	28.85	50
LUM 697	Lung (H)	32.70	97

H: Human; M: murine; R: rat.

was found to correlate with the area of PM in monolayer culture (Table I, $p<0.0029$). However, no correlation was found between PM formation and relative levels of HAS or HYAL mRNA levels. These findings suggest that the direct measurement of tumor cell-associated HA using an HABP-based assay (24) offers the most reliable predictor of PM formation. Further efforts to define the relationship between tumor-associated HA and response to agents that modify tumor stroma by depleting HA content therefore used a bHABP method combined with a digital analysis to obtain scores that were grouped as HA$^{+1,2 \text{ or } 3}$ (low to high HA).

HA accumulation predicts efficacy of PEGPH20 in diverse cell line-derived tumors. Two forms of rHuPH20 were evaluated for use in animal tumor models, unmodified rHuPH20 (25) and the pegylated form, PEGPH20 (20). While both forms have the same substrate specificity, PEGPH20 has a much longer serum half-life (20). When compared for efficacy in the H1975 NSCLC xenograft tumor model, rHuPH20 demonstrated little or no activity vs. vehicle control, while PEGPH20 led to approximately 35% tumor growth inhibition (Table III), consistent with our earlier results which showed that the PEGPH20 has an approximately 200-fold increased bioavailability compared to the parent molecule (20). PEGPH20 was then used for further *in vitro* and *in vivo* studies.

Despite its activity in animal models, PEGPH20 has no growth inhibitory activity on monolayer tumor cell cultures, regardless of the level of HA expression (20). Depletion of HA therefore appears to preferentially impact three dimensional growth, leading to the idea that growth of some tumors *in vivo* may be in part dependent upon the density and amount of HA-rich ECM (26), and furthermore, depletion of HA from HA^{+3} tumors may have a more pronounced effect on tumor growth than depletion of HA from an HA^{+1} tumor. To test this hypothesis, 14 tumor cell line-derived tumors were characterized for their HA content by histochemistry utilizing bHABP and digital imaging quantification. Despite the diversity of tumor cell types (human, murine and rat origin) there was a significant correlation ($p<0.001$) between increasing HA staining intensity and the *in vivo* antitumor activity of PEGPH20 (Figure 1 and Table IV).

To further establish the importance of HA accumulation as a criterion for antitumor response to HA depletion by PEGPH20, DU-145 prostate tumor cell line was transduced with pLXRN retrovirus encoding human HAS2, or with control pLXRN. *HAS2*-transfected DU-145 (DU-145/HAS2) displayed increased HA production and enhanced pericellular matrix formation *in vitro* (Table I). Additionally, the HAS2-overexpressing DU-145 prostate tumor xenograft grew more aggressively in nude mice than did the parental cell line transfected with empty vector (DU-145/VO), similar to previous reports by other groups (Figure 2) (26-28). Only growth of DU-145/HAS2 was inhibited following treatment with PEGPH20 (46% inhibition, Figure 2). These results support the hypothesis that accumulation of HA in the ECM enhances tumor development, and that tumors characterized by increased HA accumulation are more sensitive to the growth inhibitory effects of HA depletion.

Utility of HA as a biomarker for predicting response of human NSCLC tumors to PEGPH20. NSCLC remains difficult to treat successfully, thus there is much interest in therapeutics which target molecules that are relevant to the pathobiology of the disease. NSCLC accumulation of HA has been described (29), and worse prognosis has been associated with elevated tumor-associated HA in a subset of patients with NSCLC (29-31). To confirm the occurrence and frequency of HA accumulation in NSCLC, a panel of 190 NSCLC archived biopsies were
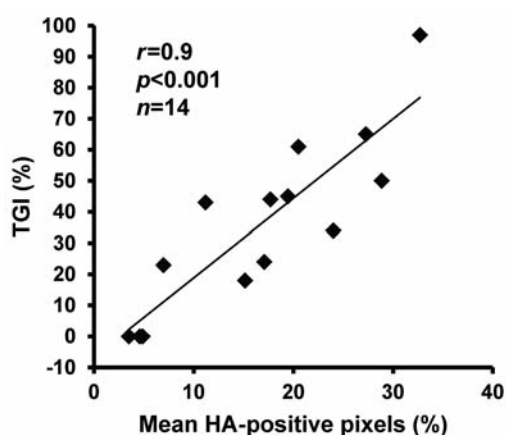
Figure 1. *Tumor HA staining intensity and corresponding pegylated recombinant human PH20 hyaluronidase (PEGPH20)-mediated growth inhibition. Tumor-bearing mice were treated with vehicle or PEGPH20 twice weekly for 2-3 weeks when tumor volumes reached ~400 mm³. At study termination, tumors were harvested and HA levels assessed histologically as described in the Materials and Methods section. Tumor growth inhibition (TGI) versus HA staining intensity. Statistical testing using Spearman's rank correlation coefficient indicates a significant correlation between HA intensity and response to PEGPH20 treatment (n=14, Spearman's r=0.9, p<0.001). Results are from tumors treated with at least 1 mg/kg of PEGPH20, which was shown to have identical TGI as those treated at higher doses (Jiang; unpublished results). Individual TGI values are given in Table IV.*

Table V. *Distribution of hyaluronan (HA) expression in human lung cancer samples.*

HA score	HA positive incidence (%)				
	ADC	SCC	LCC	Other	Normal
0	3 (4.7)	0 (0)	0 (0)	1 (3)	0 (0)
1	23 (36)	24 (25)	1 (17)	11 (48)	9 (43)
2	31 (48)	33 (34)	3 (50)	9 (39)	12 (57)
3	7 (11)	40 (41)	2 (33)	2 (8.7)	0 (0)
Total	62 (32)	99 (52)	6 (3)	23 (12)	21 (100)

HA scores were defined as described in the Materials and Methods section; ADC: Adenocarcinoma; SCC: squamous cell carcinoma; LCC: large cell carcinoma.

examined for histopathological type and HA accumulation. In this panel, adenocarcinoma (ADC), squamous cell carcinoma (SCC), and large cell carcinoma (LCC) were observed at frequencies of 32%, 52%, and 3%, respectively (Table V). Other unidentified subtypes comprised about 12% of the 190 samples examined. Forty-one percent of SCC cases displayed the HA^{+3} phenotype, while 11% of ADC and 33% of LCC cases were scored as HA^{+3}. In this dataset, no normal lung tissue samples exhibited the HA^{+3} phenotype, although HA was detected in most samples of normal lung tissue.

Our findings using tumor cell line-derived tumors in nude mice (Figure 1 and Table IV) suggest that diverse tumor types respond to PEGPH20 in relation to accumulation of HA. In order to further test the relationship between HA overexpression and antitumor response of NSCLC to PEGPH20-mediated HA depletion, we analyzed a set of human NSCLC tumor explants maintained at a low passage number in nude mice, a more clinically relevant situation than cell line-derived tumors (32, 33). Because SCC-type NSCLC had the highest percentage of HA^{+3} tumors, we utilized this subtype to test the relationship between HA accumulation and response to PEGPH20. Tumors selected for testing in nude mice were LUM858 (HA+1), LUM330 (HA^{+2}), and LUM697 (HA^{+3}). As suggested by earlier

experiments (Figure 1 and Table IV), the rank-order of HA accumulation score was predictive of the degree of TGI in animal models, with means of 16%, 44% and 97% for LUM858 (HA^{+1}), LUM330 (HA^{+2}), and LUM697 (HA^{+3}), respectively (Figure 3).

Mechanism of action of PEGPH20: inhibition of DNA synthesis in xenograft tumor cells and impact on the TME. PEGPH20-mediated HA depletion of HA^{+3} tumors results in decreased tumor water content and IFP, while increasing tumor vascular flow and perfusion of chemotherapy (10, 20, 34). Thus, depletion of HA from the tumor matrix has a major impact on tumor structural properties. However, the mechanism(s) by which HA depletion can lead to inhibition of tumor growth is not obvious. For instance, increased vascular perfusion achieved following treatment of HA^{+3} tumors with PEGPH20 alone (20) might be pro-tumorigenic by reducing tumor hypoxia. To evaluate whether HA depletion has antiproliferative effects on tumor cells *in vivo*, mice with PC3 (HA^{+3}) tumor xenografts, treated with PEGPH20 or vehicle, were administered BrdU the day before study termination. Tumor cell DNA synthesis was assessed after staining with anti-BrdU antibody. The percentage of BrdU-positive nuclei was significantly reduced from 4.8% to 2%, a 58.3% reduction in synthetically active nuclei (Figure 4A).

Many types of changes in the TME could result in reduced tumor DNA synthesis. These include increased cell–cell contact, depletion of nutrient stores from the HA-rich matrix, and significant biomechanical changes which accompany dramatically reduced tumor IFP, therefore altering the fluid pressure differential between the tumor and its external environment (20). Physical changes in the TME can impact gene expression (35), and thus we hypothesized that removal of HA might influence levels of TME proteins associated with tumor growth. We initially investigated murine collagen I (Col1α1), murine collagen V (Col5α1), and murine tenascin
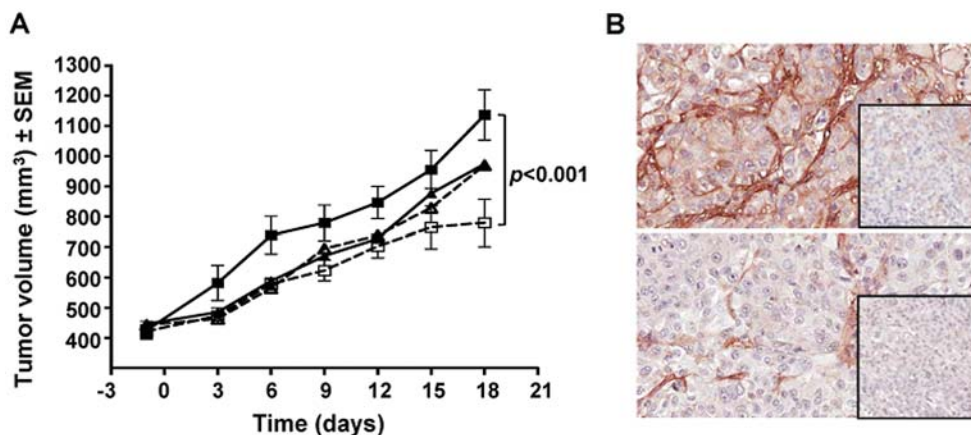
Figure 2. *Pegylated recombinant human PH20 hyaluronidase (PEGPH20) selectively inhibits tumor growth in hyaluronan (HA)-rich tumors. Mice inoculated with either DU-145/VO or DU-145/HAS2 cells were subsequently treated with vehicle alone or PEGPH20 (4.5 mg/kg, twice weekly for 3 weeks). A: Tumor volume plotted versus time (days). PEGPH20 inhibited tumor growth in DU-145/HAS2 tumors (tumor growth inhibition[TGI]=50%, p<0.001, n=8), but not in DU-145/VO tumors (TGI=0.7%, p>0.05, n=8). B: Representative micrographs of DU-145/HAS2 (top) and DU-145/VO (bottom) HA staining. Insets: Representative PEGPH20-treated tumor sections (inset magnification ×200). DU-145/HAS2 tumor treated with vehicle (■); DU-145/HAS2 tumor treated with PEGPH20 (□); DU-145/VO tumor treated with vehicle (▲); DU-145/VO tumor treated with PEGPH20 (△).*
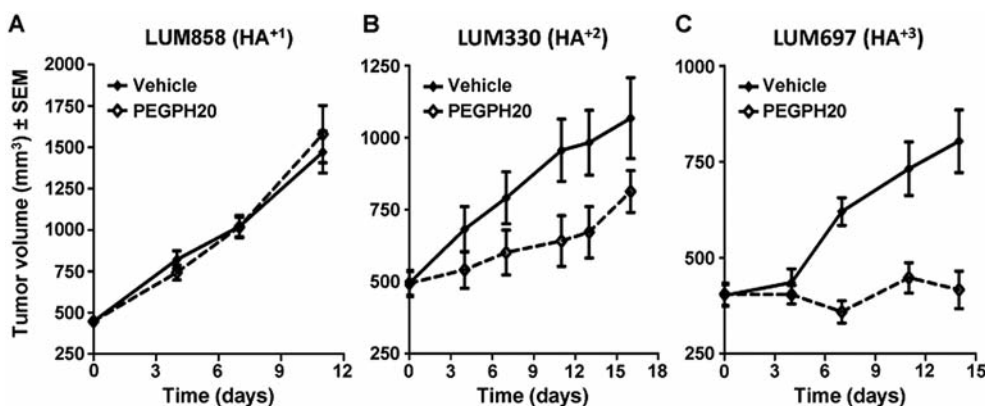

Figure 3. *Prospective analysis of hyaluronan (HA) phenotype can be used to predict response to pegylated recombinant human PH20 hyaluronidase (PEGPH20) in human tumor explants. Sixteen human non-small cell lung cancer (NSCLC) tumor explants were screened for HA phenotype and three squamous cell-type NSCLC tumors (LUM858, HA^{+1}; LUM330, HA^{+2}; LUM697, HA^{+3}) were chosen for experimental therapy with PEGPH20.*

C (Tnc), which are up-regulated in actively remodeling matrix (36). Following depletion of HA by treatment with PEGPH20, 80% tumor-specific reduction of tumor-associated collagen I was observed, as compared to stable collagen I staining in skin from treated mice (Figure 4B). Decreased levels of murine (stromal) mRNAs for Col1α1, Col5α1 and Tnc were measured by mRNA expression array analysis. Tnc mRNA decreased the most (66%), followed by Col1α1 (53%) and Col5α1 (45%; Figure 4C). These results indicate that the glycomic and proteomic aspects of the TME seem to function in a coordinated manner.

Discussion

There are several elements in the TME which are being explored for cancer therapy, including vascular endothelial growth factor (VEGF), the Wnt signaling pathway, the Hedgehog signaling pathway, and others (2, 28, 37). This report documents that enzymatic depletion of HA from the tumor stroma has an antitumor effect when the pegylated form of PH20 (PEGPH20) is used in animal models, and the degree of TGI is dependent upon the extent of accumulation of HA in the TME. Furthermore, we demonstrate that
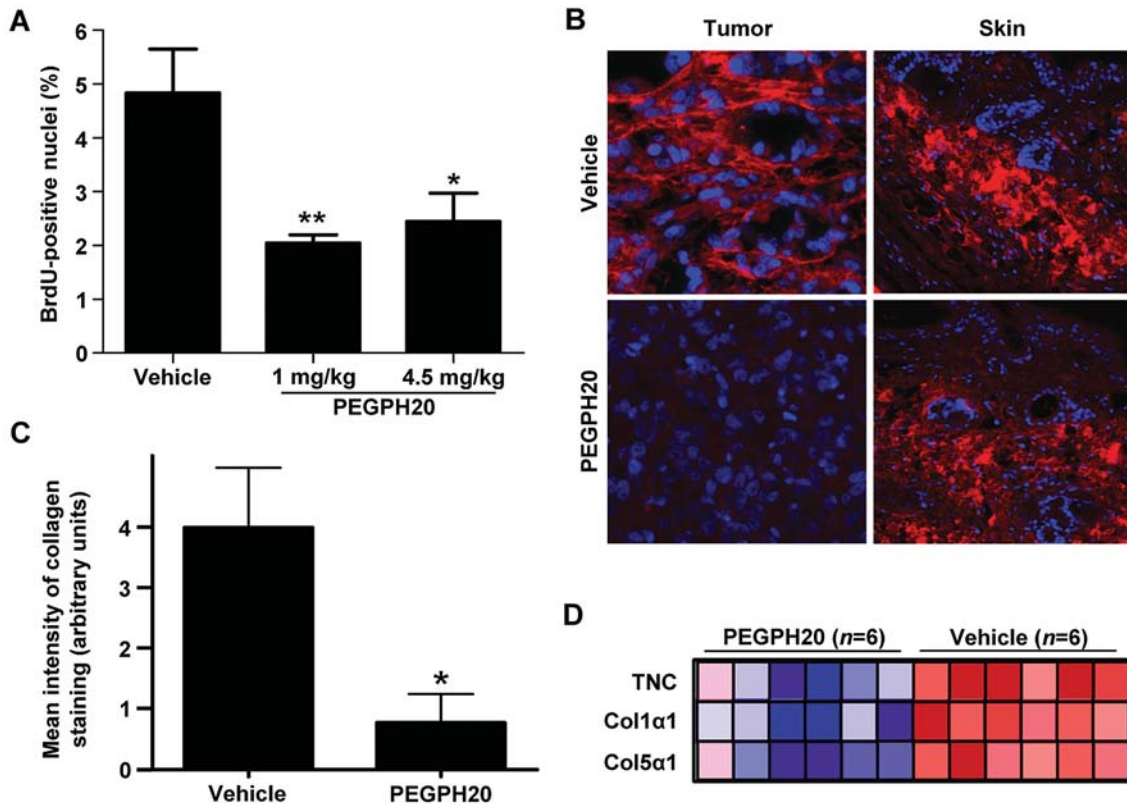
Figure 4. *Systemic pegylated recombinant human PH20 hyaluronidase (PEGPH20) administration inhibits bromodeoxyuridine (5-bromo-2'-deoxyuridine, BrdU) incorporation in vivo, and modulates expression of other extracellular matrix components. A: Relative BrdU expression in PC3 tumors treated with vehicle alone, or 1 mg/kg or 4.5 mg/kg PEGPH20 (n=5; *p<0.05, **p<0.01 compared to vehicle). B: Immunofluorescence localization of collagen I (red) in mouse skin (right panels) and PC3 tumors (left panels) treated with vehicle or 4.5 mg/kg of PEGPH20 (magnification ×400 tumor; ×200 skin). C: Image analysis of collagen staining in PC3 tumor and mouse skin following treatment with vehicle or PEGPH20 as described in the Materials and Methods section. D: Heat map of selected gene expression from Affymetrix Mouse 430 2.0 array (n=6). Tnc: Murine tenascin C; Col1α1: murine collagen I; Col5α1: murine collagen V.*

depletion of HA impacts expression of other TME components which may play a role in the antitumor effects of PEGPH20.

A semiquantifiable scoring method was developed for documenting HA expression as a TME biomarker for therapy. We compared measurements of soluble HA in cell culture media with measurement of the mRNAs encoding HAS1, -2, and -3, and HYAL1 and -2 in order to determine which of these potential markers predicted tumor cell competence to form PM *in vitro*, as a surrogate for ECM *in vivo*. Only HA determination using the glycomics probe (HABP) correlated with PM formation and HA score in cell line-derived tumors in nude mice. Other enzymes leading to synthesis of HA are the subject of future work (38).

The relationship between HA accumulation and *in vivo* response to PEGPH20 was studied in 14 tumors of human, rat and murine origin (HA^{+1} to HA^{+3}). The results showed that TGI by PEGPH20 strongly correlated with tumor HA

accumulation ($p<0.001$, Figure 1 and Table IV). To confirm the relationship between increased tumor HA and response to PEGPH20, the HA+1 DU-145 (prostate) tumor cell line was transfected with LXRN:HAS2 retroviral vector, and cell populations overexpressing HAS2 were derived by G418 selection. No significant growth inhibition by PEGPH20 was seen in xenografts derived from the control DU-145/VO tumor cell line, while growth of HAS2-transfected variants producing HA was growth inhibited *in vivo* by 46% (Figure 2).

While previous data have shown that HAS overexpression can result in more aggressive tumor growth in murine models (27, 39, 40), and that HAS inhibitors can reverse some malignant properties of tumor cells (40, 41), this is the first demonstration that HA accumulation can predict the sensitivity of a tumor to PEGPH20-mediated TGI. While the value of any biomarker rests on its successful clinical application (42), the first steps involve understanding the molecular pathology underlying the biomarker (43). The data

described above have established an assay and linked the biomarker, HA, to PEGPH20-mediated antitumor responses in animal models. Others have previously established a link between tumor HA expression and more aggressive malignancy, including a subset of NSCLC (29-31). We have confirmed this earlier work, and shown that the greatest frequency of the HA+3 phenotype in NSCLC occurs in SCC (41%, Table V). Cell line-derived tumors in nude mice have proven useful in the discovery and proof of concept for many anticancer biologics (44). However, this system has limitations, due to the lack of genetic diversity of transplantable tumors, as well as the absence of syngeneic stromal cells (32). To more directly test the possible clinical applicability of PEGPH20 in HA-stratified patients, fresh tumor explants from patients with NSCLC were characterized for HA phenotype and subsequently grown subcutaneously in nude mice. The low passage number allows these tumors to retain the genetic heterozygosity of the patient's tumor and perhaps elements of the original stroma (32, 33). From among the samples available, three SCC tumors, LUM858 (HA^{+1}), LUM330 (HA^{+2}) and LUM697 (HA+3), were transplanted into nude mice and tested for growth inhibition by PEGPH20. The results from this experiment support the predictive value of the HA biomarker for response to PEGPH20 (HA^{+3}, 97% TGI; HA^{+2}, 44% TGI; HA^{+1}, 16% TGI; Figure 3). Additional explants are currently being studied to support these initial results.

The mechanisms of inhibition of tumor growth by targeting components of the TME are likely to be complex because of the many interacting molecules present in the ECM (45). For instance, HA interacts with a family of canonical binding proteins, the hyaladherins, each of which may have an impact on stromal or malignant cell behavior (1, 46, 47). When PEGPH20 degrades HA in the ECM, these interactions and downstream interactions are disrupted. One result of HA depletion could include release of sequestered growth factors and cytokines from the TME, and increased cell–cell contact, events expected to inhibit proliferation of tumor cells. We have shown here that treatment of PC3 (HA^{+3}) xenografts with PEGPH20 does indeed have an impact on DNA synthesis (>50% inhibition, Figure 4A).

It is unclear how the depletion of one TME component may influence the synthesis and degradation of other matrix components. Surprisingly, tumor (but not skin) collagen content was reduced by 80% as determined by collagen I staining of tissue sections following HA depletion of HA+3 PC3 tumor xenografts with PEGPH20 (Figure 4C). A possible explanation for the selective nature (tumor vs. skin) of collagen I depletion could be that it is initiated as a result of the dramatic biomechanical alterations that occur when HA is depleted from an HA^{+3} tumor environment (20, 48). Consistent with reduced collagen I staining in the tumor was a decrease of murine $Col1\alpha1$ mRNA (53%). Partly surveying

the effect of HA depletion on the expression of other stromal components (49, 50), mRNA for $Col5\alpha1$ and the stromal inflammatory glycoprotein Tnc were both down-regulated following *in vivo* treatment with PEGPH20 ($Col5\alpha1$, 45%; and Tnc, 66%; Figure 4D). Removal of HA from the TME therefore may have a broad impact on expression of matrix proteins and on the biology of the tumor.

A tumor is a highly specialized structure with malignant cells, stromal cells and ECM all co-evolving (45). The TME is of vital importance for tumor growth and spread, and here we document that depletion of a single ECM component, HA, leads to significant effects on tumor growth. The responsiveness to depletion of HA by PEGPH20 correlated with the degree of HA expression detected by semiquantitative histochemistry based upon bHABP, and thus provides a potential biomarker to select patients most likely to have successful therapy with PEGPH20. Partial evaluation of the mechanism of TGI revealed reduction in synthesis of other matrix components, $Col1\alpha1$, $Col5\alpha1$, as well as Tnc. Taken together, this study provides a rationale for exploring the potential of targeting the tumor microenvironment in human cancer clinically, and specifically the HA component of HA^{+3} malignancies, as a therapeutic modality that should be additive or perhaps synergistic with directly targeting the malignant cells.

Declaration of Interests

Acknowledgements

References

1 Järveläinen H, Sainio A, Koulu M, Wight TN and Penttinen R: Extracellular matrix molecules: potential targets in pharmacotherapy. Pharmacol Rev *61*: 198-223, 2009.

2 Whatcott CJ, Han H, Posner RG, Hostetter G and Von Hoff DD: Targeting the tumor microenvironment in cancer: Why hyaluronidase deserves a second look. Cancer Discov *1*: 291-296, 2011.

3 Tammi RH, Kultti A, Kosma VM, Pirinen R, Auvinen P and Tammi MI: Hyaluronan in human tumors: pathobiological and prognostic messages from cell-associated and stromal hyaluronan. Semin Cancer Biol *18*: 288-295, 2008.

4 Bouzin C and Feron O: Targeting tumor stroma and exploiting mature tumor vasculature to improve anticancer drug delivery. Drug Resist Updat *10*: 109-120, 2007.

5 Kinsella MG, Bressler SL and Wight TN: The regulated synthesis of versican, decorin, and biglycan: extracellular matrix proteoglycans that influence cellular phenotype. Crit Rev Eukaryot Gene Expr *14*: 203-234, 2004.

6 Oikonomopoulou K, Diamandis EP and Hollenberg MD: Kallikrein-related peptidases: proteolysis and signaling in cancer, the new frontier. Biol Chem 391: 299-310, 2010.

7 Rugg MS, Willis AC, Mukhopadhyay D, Hascall VC, Fries E, Fülöp C, Milner CM and Day AJ: Characterization of complexes formed between TSG-6 and inter-alpha-inhibitor that act as intermediates in the covalent transfer of heavy chains onto hyaluronan. J Biol Chem 280: 25674-25686, 2005.

8 Itano N, Zhuo L and Kimata K: Impact of the hyaluronan-rich tumor microenvironment on cancer initiation and progression. Cancer Sci 99: 1720-1725, 2008.

9 Camenisch TD, Spicer AP, Brehm-Gibson T, Biesterfeldt J, Augustine ML, Calabro A Jr., Kubalak S, Klewer SE and McDonald JA: Disruption of hyaluronan synthase-2 abrogates normal cardiac morphogenesis and hyaluronan-mediated transformation of epithelium to mesenchyme. J Clin Invest 106: 349-360, 2000.

10 Eikenes L, Tufto I, Schnell EA, Bjørkøy A and De Lange Davies C: Effect of collagenase and hyaluronidase on free and anomalous diffusion in multicellular spheroids and xenografts. Anticancer Res 30: 359-368, 2010.

11 Bollyky PL, Wu RP, Falk BA, Lord JD, Long SA, Preisinger A, Teng B, Holt GE, Standifer NE, Braun KR, Xie CF, Samuels PL, Vernon RB, Gebe JA, Wight TN and Nepom GT: ECM components guide IL-10 producing regulatory T-cell (TR1) induction from effector memory T-cell precursors. Proc Natl Acad Sci USA 108: 7938-7934, 2011.

12 Godar S, Ince TA, Bell GW, Feldser D, Donaher JL, Bergh J, Liu A, Miu K, Watnick RS, Reinhardt F, McAllister SS, Jacks T and Weinberg RA: Growth-inhibitory and tumor-suppressive functions of p53 depend on its repression of CD44 expression. Cell 134: 62-73, 2008.

13 Sohr S and Engeland K: RHAMM is differentially expressed in the cell cycle and down-regulated by the tumor suppressor p53. Cell Cycle 7: 3448-3460, 2008.

14 Granger HJ, Laine SH and Laine GA: Osmotic pressure exerted by entangled polysaccharide chains. Microcirc Endothelium Lymphatics 2: 85-105, 1985.

15 Granger DN, Barrowman JA, Harper SL, Kvietys PR and Korthuis RJ: Sympathetic stimulation and intestinal capillary fluid exchange. Am J Physiol 247: G279-283, 1984.

16 Granger HJ, Laine GA, Barnes GE and Lewis RE: Dynamics and control of transmicrovascular fluid exchange. *In*: Edema. (Staub NC and Taylor AE (eds.). New York, Raven Press, pp. 189-228, 1984.

17 Chow G, Tauler J and Mulshine JL: Cytokines and growth factors stimulate hyaluronan production: role of hyaluronan in epithelial to mesenchymal-like transition in non-small cell lung cancer. J Biomed Biotechnol 2010: 485468; 1-11, 2010.

18 Sironen RK, Tammi M, Tammi R, Auvinen PK, Anttila M and Kosma VM: Hyaluronan in human malignancies. Exp Cell Res 317: 383-391, 2011.

19 Li L, Asteriou T, Bernert B, Heldin CH and Heldin P: Growth factor regulation of hyaluronan synthesis and degradation in human dermal fibroblasts: importance of hyaluronan for the mitogenic response of PDGF-BB. Biochem J 404: 327-336, 2007.

20 Thompson CB, Shepard HM, O'Connor PM, Kadhim S, Jiang P, Osgood RJ, Bookbinder LH, Li X, Sugarman BJ, Connor RJ, Nadjsombati S and Frost GI: Enzymatic depletion of tumor hyaluronan induces antitumor responses in preclinical animal models. Mol Cancer Ther 9: 3052-3064, 2010.

21 Wang C, Tammi M, Guo H and Tammi R: Hyaluronan distribution in the normal epithelium of esophagus, stomach, and colon and their cancers. Am J Pathol 148: 1861-1869, 1996.

22 Volpi N: High-performance liquid chromatography and on-line mass spectrometry detection for the analysis of chondroitin sulfates/hyaluronan disaccharides derivatized with 2-aminoacridone. Anal Biochem 397: 12-23, 2010.

23 Haserodt S, Aytekin M and Dweik RA: A comparison of the sensitivity, specificity, and molecular weight accuracy of three different commercially available hyaluronan ELISA-like assays. Glycobiology 21: 175-183, 2011.

24 Hellström S, Tengblad A, Johansson C, Hedlund U and Axelsson E: An improved technique for hyaluronan histochemistry using microwave irradiation. Histochem J 22: 677-682, 1990.

25 Frost GI: Recombinant human hyaluronidase (rHuPH20): an enabling platform for subcutaneous drug and fluid administration. Expert Opin Drug Deliv 4: 427-440, 2007.

26 Itano N, Atsumi F, Sawai T, Yamada Y, Miyaishi O, Senga T, Hamaguchi M and Kimata K: Abnormal accumulation of hyaluronan matrix diminishes contact inhibition of cell growth and promotes cell migration. Proc Natl Acad Sci USA 99: 3609-3614, 2002.

27 Jacobson A, Rahmanian M, Rubin K and Heldin P: Expression of hyaluronan synthase 2 or hyaluronidase 1 differentially affect the growth rate of transplantable colon carcinoma cell tumors. Int J Cancer 102: 212-219, 2002.

28 Josefsson A, Adamo H, Hammarsten P, Granfors T, Stattin P, Egevad L, Laurent AE, Wikström P and Bergh A: Prostate cancer increases hyaluronan in surrounding nonmalignant stroma, and this response is associated with tumor growth and an unfavorable outcome. Am J Pathol 179: 1961-1968, 2011.

29 Hernández JR, García JM, Martínez Muñíz MA, Allende Monclus MT and Ruibal Morell A: Clinical utility of hyaluronic acid values in serum and bronchoalveolar lavage fluid as tumor marker for bronchogenic carcinoma. Int J Biol Markers 10: 149-155, 1995.

30 Pirinen R, Tammi R, Tammi M, Hirvikoski P, Parkkinen JJ, Johansson R, Böhm J, Hollmén S and Kosma VM: Prognostic value of hyaluronan expression in non-small cell lung cancer: Increased stromal expression indicates unfavorable outcome in patients with adenocarcinoma. Int J Cancer 95: 12-17, 2001.

31 Ohashi R, Takahashi F, Cui R, Yoshioka M, Gu T, Sasaki S, Tominaga S, Nishio K, Tanabe KK and Takahashi K: Interaction between CD44 and hyaluronate induces chemoresistance in non-small cell lung cancer cell. Cancer Lett 252: 225-234, 2007.

32 Giovanella BC, Vardeman DM, Williams LJ, Taylor DJ, de Ipolyi PD, Greeff PJ, Stehlin JS, Ullrich A, Cailleau R, Slamon DJ and Gary HE: Heterotransplantation of human breast carcinomas in nude mice. Correlation between successful heterotransplants, poor prognosis and amplification of the HER-2/neu oncogene. Int J Cancer 47: 66-71, 1991.

33 Pegram M and Ngo D: Application and potential limitations of animal models utilized in the development of trastuzumab (Herceptin): a case study. Adv Drug Deliv Rev 58: 723-734, 2006.

34 Eikenes L, Tari M, Tufto I, Bruland OS and de Lange Davies C: Hyaluronidase induces a transcapillary pressure gradient and improves the distribution and uptake of liposomal doxorubicin (Caelyx) in human osteosarcoma xenografts. Br J Cancer 93: 81-88, 2005.

35 Shieh AC: Biomechanical forces shape the tumor micro-environment. Ann Biomed Eng *39*: 1379-1389, 2011.

36 Hagedorn H, Sauer U, Schleicher E and Nerlich A: Expression of TGF-beta 1 protein and mRNA and the effect on the tissue remodeling in laryngeal carcinomas. Anticancer Res *19*: 4265-4272, 1999.

37 Hiscox S, Barrett-Lee P and Nicholson RI: Therapeutic targeting of tumor–stroma interactions. Expert Opin Ther Targets *15*: 609-621, 2011.

38 Clarkin CE, Allen S, Wheeler-Jones CP, Bastow ER and Pitsillides AA: Reduced chondrogenic matrix accumulation by 4-methylumbelliferone reveals the potential for selective targeting of UDP-glucose dehydrogenase. Matrix Biol *30*: 163-168, 2011.

39 Okuda H, Kobayashi A, Xia B, Watabe M, Pai SK, Hirota S, Xing F, Liu W, Pandey PR, Fukuda K, Modur V, Ghosh A, Wilber A and Watabe K.: Hyaluronan synthase (HAS)2 promotes tumor progression in bone by stimulating the interaction of breast cancer stem-like cells with macrophages and stromal cells. Cancer Res *72*: 537-547, 2012.

40 Itano N and Kimata K: Altered hyaluronan biosynthesis in cancer progression. Semin Cancer Biol *18*: 268-274, 2008.

41 Lokeshwar VB, Lopez LE, Munoz D, Chi A, Shirodkar SP, Lokeshwar SD, Escudero DO, Dhir N and Altman N: Antitumor activity of hyaluronic acid synthesis inhibitor 4-methylumbelli-ferone in prostate cancer cells. Cancer Res *70*: 2613-2623, 2010.

42 Wolff AC, Hammond ME, Schwartz JN, Hagerty KL, Allred DC, Cote RJ, Dowsett M, Fitzgibbons PL, Hanna WM, Langer A, McShane LM, Paik S, Pegram MD, Perez EA, Press MF, Rhodes A, Sturgeon C, Taube SE, Tubbs R, Vance GH, van de Vijver M, Wheeler TM and Hayes DF: American Society of Clinical Oncology/College of American Pathologists guideline recommendations for human epidermal growth factor receptor 2 testing in breast cancer. Arch Pathol Lab Med *131*: 18-43, 2007.

43 Shepard HM, Brdlik CM and Schreiber H: Signal integration: a framework for understanding the efficacy of therapeutics targeting the human EGFR family. J Clin Invest *118*: 3574-3581, 2008.

44 Shepard HM, Lewis GD, Sarup JC, Fendly BM, Maneval D, Mordenti J, Figari I, Kotts CE, Palladino MA Jr, Ullrich A and Slamon D: Monoclonal antibody therapy of human cancer: taking the HER2 protooncogene to the clinic. J Clin Immunol *11*: 117-127, 1991.

45 Bissell MJ, Hines WC: Why don't we get more cancer? A proposed role of the microenvironment in restraining cancer progression. Nat Med *17*: 320-329, 2011.

46 Gandhi NS and Mancera RL: The structure of glycosamino-glycans and their interactions with proteins. Chem Biol Drug Des *72*: 455-482, 2008.

47 Spencer VA, Xu R and Bissell MJ: Gene expression in the third dimension: the ECM–nucleus connection. J Mammary Gland Biol Neoplasia *15*: 65-71, 2010.

48 Asparuhova MB, Ferralli J, Chiquet M and Chiquet-Ehrismann R: The transcriptional regulator megakaryoblastic leukemia-1 mediates serum response factor-independent activation of tenascin-C transcription by mechanical stress. FASEB J *25*: 3477-3488, 2011.

49 Udalova IA, Ruhmann M, Thomson SJ and Midwood KS: Expression and immune function of tenascin-C. Crit Rev Immunol *31*: 115-145, 2011.

50 Chiquet M, Gelman L, Lutz R and Maier S: From mechanotransduction to extracellular matrix gene expression in fibroblasts. Biochim Biophys Acta *1793*: 911-920, 2009.

51 Udabage L, Brownlee GR, Nilsson SK and Brown TJ: The over-expression of HAS2, HYAL-2 and CD44 is implicated in the invasiveness of breast cancer. Exp Cell Res *310*: 205-217, 2005.